Role of Coulomb interactions in dark-bright magnetoexciton mixing in strained quantum wells

Y. D. Jho,[1,3] F. V. Kyrychenko,[1] J. Kono,[2] X. Wei,[3] S. A. Crooker,[4] G. D. Sanders,[1] D. H. Reitze,[1] C. J. Stanton,[1] and G. S. Solomon[5]

[1]*Department of Physics, University of Florida, Gainesville, Florida 32611, USA*
[2]*Department of Electrical and Computer Engineering, Rice University, Houston, Texas 77005, USA*
[3]*National High Magnetic Field Laboratory, Florida State University, Tallahassee, Florida 32310, USA*
[4]*National High Magnetic Field Laboratory, Los Alamos National Laboratory, Los Alamos, New Mexico 87545, USA*
[5]*Solid-State Laboratories, Stanford University, Stanford, California 94305, USA*
(Received 13 October 2004; revised manuscript received 24 March 2005; published 19 July 2005)

Coupled magnetoexciton states between allowed ("bright") and forbidden ("dark") transitions are found in absorption spectra of strained $In_{0.2}Ga_{0.8}As/GaAs$ quantum wells with increasing magnetic field up to 30 T. We find large (~9 meV) energy splittings in the mixed states. The observed anticrossing behavior is independent of polarization, and sensitive only to the parity of the quantum confined states. Detailed experimental and theoretical investigations indicate that valence band complexity does not play a role. We find that the excitonic Coulomb interaction is a necessary condition for the anticrossing to occur, while the magnitude of the energy splitting correlates with strain. In addition, we determine the spin composition of the mixed states.

I. INTRODUCTION

When energy levels of excited states are tuned to the same energy, one can observe either crossing or anticrossing behavior, depending on the coupling character of the external perturbations.[1] If the coupling matrix element of perturbing terms is nonvanishing, their corresponding wave functions are mixed so that the crossing is suppressed and replaced by anticrossing behavior. In semiconductor heterostructures, valence-band complexity (i.e., $\mathbf{k} \cdot \mathbf{p}$ interactions in confined geometries arising from spin-orbit coupling) has been extensively investigated in GaAs-based quantum wells (QWs) and proposed as the main coupling mechanism.[2–7] Due to the relatively small heavy-hole–light-hole (HH-LH) separation and resulting close proximity of valence band manifolds, the coupling of HH-LH exciton states in GaAs QWs can be substantiated through strong modifications of in-plane effective masses[8,9] and transitions that are nominally forbidden in a simple two-band model can be observed optically.[4–6,10] While a number of studies on valence-band complexity have been reported for exciton-mixing in QWs, it is conceivable that other mechanisms can also determine the nature of the interaction. Recently, anticrossing involving bright and dark excitons in single quantum dot molecules due to coherent coupling between the states of the two dots has been observed.[11] In addition, large splittings of cyclotron resonance lines in $Al_xGa_{1-x}N/GaN$ heterostructures have been reported,[12] however, the origins of anticrossing interactions in high magnetic fields are not completely understood.

As a way to investigate whether exciton mixing is significantly influenced by other mechanisms, indium can be incorporated into the QW layer to induce strain. Since the lattice constant of $In_xGa_{1-x}As$ QW is larger than that of surrounding GaAs layers, a biaxial compressive strain is introduced. This strain tensor can be decomposed into a uniaxial and a hydrostatic component. The hydrostatic component shifts the band gap energies while the uniaxial strain induces large valence-band offset.[13] Most importantly, the uniaxial deformation potential also lowers the LH energy relative to the HH energy,[14] thereby reducing the hole-level coupling and its corresponding repulsive interaction between LH and HH subbands.[9] Thus, one can minimize the effects of valence band complexity in $In_xGa_{1-x}As$ QWs and obtain discrete optical spectra of HH and LH excitons in the high magnetic field regime. In addition, QWs provide lighter in-plane masses of HHs than that of LHs,[7,15,16] and therefore the magnetoexciton sublevels evolve differently in applied magnetic fields.[3,8,17] Thus, $In_xGa_{1-x}As/GaAs$ QWs are ideally suited for exploring the nature of the mixing interaction. Although several groups have explored the nature of magnetoexcitons in bulk and quantum well systems both theoretically[3,17,18] and experimentally,[19,20] no studies have explicitly been directed at the $In_xGa_{1-x}As/GaAs$ system as a way to reduce the influence of valence band complexity.

In this paper, we report on the observation of coupled states between forbidden and allowed interband transitions in strained $In_xGa_{1-x}As$ QW structures in strong magnetic fields (up to 30 T). A kind of mixed magnetoexciton state is found in a system where the anticrossing between hole states itself is suppressed. We show experimentally and theoretically that the anticrossing does not arise from valence band complexity but requires the presence of the Coulomb interaction. However, the magnitude of the energy splitting is larger than that predicted by a simple model incorporating Coulomb interactions, indicating that other mechanisms such as axial (in-plane) strain also play a role.

The paper is organized as follows. In Sec. II, we discuss the experimental and theoretical methods used in our investigations. Magnetoabsorption and photoluminescence data are presented in Sec. III. These data are compared with two theoretical models, one which accounts only for valence band complexity through the $\mathbf{k} \cdot \mathbf{p}$ interaction and one which incorporates the Coulomb interaction. In Sec. IV, we analyze the spin character of the mixed states. We summarize our findings in Sec. V.

II. EXPERIMENTAL AND THEORETICAL METHODS

A. Experimental methods

Experiments were performed on two $In_{0.2}Ga_{0.8}As/GaAs$ quantum well samples, consisting of 15 layers of 8-nm-thick QWs separated by 15-nm GaAs barriers, grown by molecular beam epitaxy at 430 °C (S1) and 390 °C (S2). To investigate the character of mixed states at low densities, absorption measurements were carried out in $In_{0.2}Ga_{0.8}As/GaAs$ multiple quantum wells for σ^- and σ^+ polarizations at 4.2 K. In order to minimize sample-dependent effects, two samples were studied to elucidate the common features of the exciton mixing. Magnetic fields were applied perpendicular to the QW plane. Care was taken to ensure that the planes of the quantum wells were perpendicular to the magnetic field direction to better than 1°. Most of our experiments were conducted up to field strengths of 30 T using a resistive Bitter-type magnet at the National High Magnetic Field Laboratory. White light from a tungsten lamp was used as the excitation source to investigate magnetoabsorption in the low carrier density regime. Both excitation and collection were performed through an optical fiber at normal incidence to the sample surface. In order to investigate exciton mixing at higher carrier densities, we also performed magnetophotoluminescence on our sample as a function of excitation power. For these experiments, a linearly polarized 150 fs, 775 nm pulse from a chirped pulse amplifier (Clark-MXR CPA-2001) was focused through free space to a $500\mu m$ spot on the sample. Unpolarized PL was collected using a fiber optic probe from the backside of the sample and examined as a function of both magnetic field and excitation power.

B. Theoretical methods

Two distinct theoretical approaches were taken to provide a framework for analyzing our data. The first approach is based on $\mathbf{k}\cdot\mathbf{p}$ theory and the Pidgeon-Brown model,[21,22] explicitly incorporating the full valence band complexity but not including excitonic effects arising from the Coulomb interaction. In the second approach, we use a treatment based on the Bauer-Ando formalism[3] but modified to be valid at high magnetic fields.

For the discussions that follow, we use the high-field Landau notation to specify a quantum well exciton state in a magnetic field (as opposed to the low-field excitonic notation); for low-field–high-field correspondence, see, e.g., Ref. 23. Each state has four indices, i.e., N, M, n_e, and n_h (or n_l). Here N and M are electron and hole Landau quantum numbers, respectively $(N, M = 0, 1, 2, \ldots)$. The electron and HH (LH) QW energy levels are denoted by n_e and n_h (n_l). For the present work, the most relevant QW level indices are $n_e = 1$ and 2, $n_h = 1$, 2, and 3, and $n_l = 1$. For convenience, we neglect the spin index and center-of-mass momentum of each magnetoexciton state. We denote bright (i.e., optically active) HH (LH) exciton states $|N, M, n_e, n_h(n_l)\rangle = |N, N, n, n\rangle$ as Hn^N (Ln^N) and dark (i.e., optically inactive) HH exciton states $|N, M, n_e, n_h\rangle = |N, N, 1, n_h(\neq 1)\rangle$ as Dn^N. Thus, all the dark states we are considering here are associated with $n_e = 1$ electrons; note also that within the spherical approximation the

Landau quantum number is always conserved $(N = M)$.

1. Valence band complexity in the absence of the Coulomb interaction

Our model for magnetoabsorption in a superlattice is based on a modified eight band Pidgeon-Brown model explicitly incorporating pseudomorphic strain in the superlattice bandstructure. The details of the calculation can be found in Ref. 22; we summarize the salient features here. Eight Bloch basis states are separated into an upper and lower set which decouple at $k_z = 0$. Assuming that the magnetic field B is oriented along the z axis and working in the Landau gauge, the bulk effective mass Hamiltonian is written as the sum of the Landau and strain contributions

$$H = H_L + H_S, \tag{1}$$

where the elements of H_L are functions of the band gap E_g, the modified Luttinger parameters,[24] the Kane momentum matrix element, and the magnetic length $\lambda = \sqrt{\hbar c / eB} = \sqrt{\hbar^2 / 2m_0 \mu_B B}$.[25] The elements of H_S are functions of the strain tensor components and deformation potentials of InAs and GaAs.

The envelope function of the effective mass Hamiltonian (1) in the superlattice can be written as

$$\mathcal{F}_{n,\nu} = \frac{e^{i(k_y y + k_z z)}}{\sqrt{\mathcal{A}}} \begin{bmatrix} U_{n,1,k_z,\nu}(z)\phi_{n-1} \\ U_{n,2,k_z,\nu}(z)\phi_{n-2} \\ U_{n,3,k_z,\nu}(z)\phi_{n} \\ U_{n,4,k_z,\nu}(z)\phi_{n} \\ U_{n,5,k_z,\nu}(z)\phi_{n} \\ U_{n,6,k_z,\nu}(z)\phi_{n+1} \\ U_{n,7,k_z,\nu}(z)\phi_{n-1} \\ U_{n,8,k_z,\nu}(z)\phi_{n-1} \end{bmatrix}, \tag{2}$$

where n is the Landau quantum number associated with the Hamiltonian matrix, ν labels the eigenvectors, $\mathcal{A} = L_x L_y$ is the cross sectional area of the sample in the xy plane, $\phi_n(\xi)$ are harmonic oscillator eigenfunctions evaluated at $\xi = x - \lambda^2 k_y$, and $U_{n,m,k_z,\nu}(z)$ are eight complex envelope functions ($m = 1, \ldots, 8$) for the νth eigenstate. A finite difference scheme is used to obtain the energies and wave functions in the superlattice. Substituting $\mathcal{F}_{n,\nu}$ from Eq. (2) into the effective mass Schrödinger equation with H given by Eq. (1), we obtain a matrix eigenvalue equation

$$H_n F_{n,\nu} = E_{n,\nu}(k_z) F_{n,\nu}, \tag{3}$$

that can be solved for each allowed value of the Landau quantum number n and wave vector k_z to obtain eigenvalues and eigenvectors. The resulting eigenvalues are the Landau levels, denoted $E_{n,\nu}(k_z)$, where n labels the Landau level and ν labels the eigenenergies belonging to the same Landau level in ascending order. The corresponding eigenvectors $F_{n,\nu}$ are the cell periodic functions $U_{n,m,k_z,\nu}(z_i)$ evaluated at the grid points z_i.

While this model explicitly incorporates pseudomorphic strain in the superlattice band structure through H_S, excitonic

TABLE I. Material parameters for InAs and GaAs.

Parameter	InAs	GaAs
Energy gap		
E_g (eV, $T=0$)	0.417[a]	1.519[a]
α (meV/K)	0.276[a]	0.5405[a]
β (K)	93[a]	204[a]
Electron effective mass		
m_e^*/m_0 ($T=0$)	0.026[a](0.022)[b]	0.067[a]
Luttinger parameters		
γ_1^L	20.0[a]	6.98[a]
γ_2^L	8.5[a]	2.06[a]
γ_3^L	9.2[a]	2.93[a]
Spin-orbit splitting		
Δ (eV)	0.39[a]	0.341[a]
Optical matrix parameters		
E_p (eV)	21.5[a]	28.8[a]
Kane parameter		
F ($T=0$)	−2.9[a]	−1.94[a]
Deformation potentials		
a_c (eV)	−5.68[a]	−7.17[a]
a_v (eV)	1.0[a]	1.16[a]
b (eV)	−1.8[a]	−2.0[a]
Elastic constants		
c_{11} (GPa)	832.9[a]	1221[a]
c_{12} (GPa)	452.6[a]	566[a]
Refractive index		
n_r	3.42[c]	3.4[c]

[a]Reference 29.
[b]Reference 22.
[c]Reference 33.

effects resulting from the Coulomb interaction are not included. In these calculations, the conduction band offset is taken to be 0.7 of the total band offset and the strain in the wells is determined by the average lattice constant in the superlattice while the barrier lattice constant is pinned to the substrate lattice constant.[26]

We calculate the magneto-optical absorption coefficient at a photon energy $\hbar\omega$ from[27]

$$\alpha(\hbar\omega) = \frac{\hbar\omega}{(\hbar c)n_r}\epsilon_2(\hbar\omega), \qquad (4)$$

where $\epsilon_2(\hbar\omega)$ is the imaginary part of the dielectric function and n_r is the index of refraction. The imaginary part of the dielectric function is found using Fermi's golden rule.

The material parameters we use for the InGaAs wells and the GaAs barriers are shown in Table I. For the temperature-dependent energy gap $E_g(T)$, we use the empirical Varshni formula.[28] The InAs electron mass used in our model is taken to be 0.022. The value of 0.022 for the InAs electron mass is consistent with recent cyclotron resonance measurements taken on InAs and analyzed in Ref. 22 using a bulk version of our eight band $\mathbf{k}\cdot\mathbf{p}$ model. Finally, for the In$_{0.2}$Ga$_{0.8}$As

alloy, material parameters are interpolated from InAs and GaAs values using bowing parameters as described in Ref. 29.

2. Modified Bauer-Ando theory for high magnetic fields

The incorporation of the Coulomb interaction is accomplished by modifiying the theory of Bauer and Ando[3] for high magnetic fields. In magnetic fields, the excitonic Hamiltonian acquires explicit dependence on the electron and hole coordinates through the vector potential. Although this seemingly precludes the free center of mass motion of the exciton, a standard gauge transformation reduces the initial magnetoexciton problem to a solution of the Schrödinger equation[30–32]

$$\left[\hat{T}_e(\hat{\mathbf{k}}_e) + \hat{T}_h(\hat{\mathbf{k}}_h) + V_e(z_e) + V_h(z_h) - \frac{e^2}{\varepsilon\sqrt{r^2 + (z_e - z_h)^2}}\right]\Psi$$
$$= E\Psi, \qquad (5)$$

with

$$\hat{\mathbf{k}}_e^\parallel = \mathbf{K} - i\frac{\partial}{\partial\mathbf{r}} + \frac{e}{2\hbar c}\mathbf{B}\times\mathbf{r}, \quad \hat{k}_e^z = -i\frac{\partial}{\partial z_e},$$

$$\hat{\mathbf{k}}_h^\parallel = \mathbf{K} + i\frac{\partial}{\partial\mathbf{r}} + \frac{e}{2\hbar c}\mathbf{B}\times\mathbf{r}, \quad \hat{k}_h^z = -i\frac{\partial}{\partial z_h}.$$

Note that Eq. (5) involves only the electron-hole relative coordinate $\mathbf{r}$ in the plane of the quantum well and formally is a one-particle equation. The $\hat{T}_e$ and $\hat{T}_h$ are the electron and hole kinetic energies and, in general, are expressed by multiband Hamiltonians. The in-plane wave vector $\mathbf{K}$ describes the center-of-mass motion. Since the main contribution to the optical transitions comes from the excitons at rest, we seek solutions of Eq. (5) with $\mathbf{K}=0$.

We solve Eq. (5) by expanding the wave function in a large basis and then diagonalizing the corresponding Hamiltonian matrix. The general form of the wave function is then

$$\Psi = \sum_{s,s',i,j,n} A_{i,j,n}^{s,s'}\psi_i(z_e)\chi_j(z_h)\phi_n(\mathbf{r})|s\rangle|s'\rangle, \qquad (6)$$

where $|s\rangle$ and $|s'\rangle$ label electron and hole Bloch amplitudes.

To ensure the fast convergence of the sum (6) at low fields, one can use the solutions of the two-dimensional exciton problem as a basis set.[3] This basis provides fast convergence in the case of relatively weak magnetic fields (when the cyclotron energy is much smaller than the exciton binding energy), however, this basis set is only appropriate for magnetic fields up to 10 T. For stronger magnetic fields, we choose as a basis solutions of the problem without Coulomb interaction. A similar approach was explored in Ref. 17, where the product of electron and hole Landau level wave functions was used as a basis. However, Eq. (5) is essentially one-particle for in-plane motion, suggesting the possibility to choose a "one-particle" basis which depends only on relative coordinate $\mathbf{r}$. In addition, the calculations in Ref. 17 were performed in the Landau gauge which does not allow us to fully explore the axial symmetry of the problem.
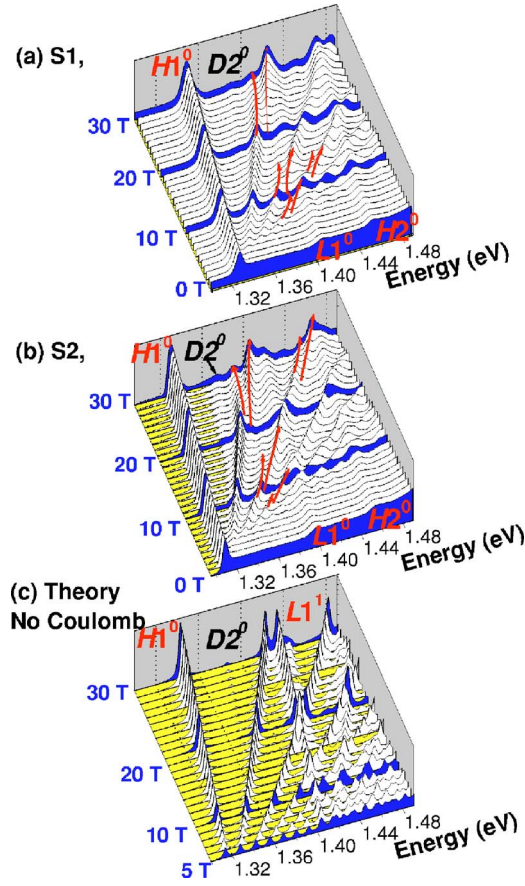
FIG. 1. (Color online.) (a), (b) Experimental magnetoabsorption spectra for $In_{0.2}Ga_{0.8}As/GaAs$ multiple quantum wells with σ^- polarization at 4.2 K for various fields up to 30 T. At zero field, three prominent peaks, indicated by $H1^0$, $L1^0$, and $H2^0$, are lowest HH exciton, lowest LH exciton, and second lowest HH exciton state, respectively. The lines $D2^0$ and $D2^1$ are assigned to the lowest and second lowest "dark" magnetoexcitons associated with the $n_e=1$ electrons and $n_h=2$ heavy holes. The arrows are guides to the eye for separated magnetoexciton peaks. (c) Theoretical absorption spectra computed using an eight band Pidgeon-Brown effective mass model. The dark state $D2^0$ is clearly visible in the spectra above 20 T.

In our model as a basis for in-plane motion we use "one-particle" functions $\phi_n(\mathbf{r})$, calculated in the symmetric gauge, where the projection of angular momentum on the field direction is a good quantum number. As a basis in the z direction, we use the set of harmonic oscillator wave functions with a nonlinear variational parameter. For conduction electrons, we assume a simple parabolic kinetic energy while for holes we use the Luttinger Hamiltonian[24] in the axial approximation. The electron effective mass, Luttinger parameters, deformation potentials, and elastic constants used are the same as those used in the Pidgeon-Brown model and are listed in Table I.

III. EXPERIMENTAL RESULTS

Figures 1(a) and 1(b) display a series of representative absorption spectra as a function of magnetic field for the case
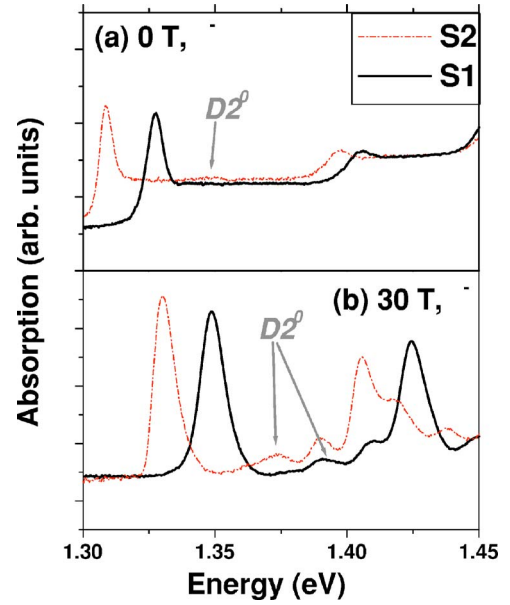

FIG. 2. (Color online.) (a) Absorption spectra at (a) zero field and (b) 30 T for samples $S1$ and $S2$ for σ^- polarization. At zero field, only HH and LH excitons are present in $S1$, while $S2$ also shows a weak dark state $D2$. In contrast, the high field absorption spectra display much stronger dark exciton states in both samples.

of σ^- polarization for $S1$ and $S2$. Note that at zero field, the HH and LH splitting is large (approaching 100 meV in both cases). As the field is increased, four effects are observed: (1) the absorption spectrum evolves from a steplike two-dimensional to a delta-function-like zero-dimensional density of states, (2) the magnetoexciton levels are resolved up to $N=6$ ($N=2$) for the HH (LH) excitons, (3) the dark state $D2^N$ develops into a clearly resolved distinct peak, and (4) significantly, the $H1^N$ subbands with $N \geqslant 1$ split into two lines [indicated by the arrows in Figs. 1(a) and 1(b)]. The energy at which the splitting occurs is found to be roughly the same distance below $L1^0$ for each state and is independent of polarization. The observation of the normally parity-forbidden $D2^0$ transition arises from the broken inversion symmetry in the presence of the magnetic field. Figure 1(c) shows the theoretically computed magneto-absorption spectra using the Pidgeon-Brown model corresponding to the experimental situation in Fig. 1(a). This theory reproduces the experimental features reasonably well, with one exception, namely, that there is no evidence of anticrossing of the $H1^N$-$D3^0$ and $H1^N$-$D3^1$ states.

In an ideal quantum well with infinite barriers, interband transitions occur only when $N=M$ and $n_e=n_h$ (n_l). However, $n_e \neq n_h$ (n_l) ("dark") transitions are usually weakly allowed in real quantum wells due to finite barrier size, lack of inversion symmetry, and perturbations such as strain or valence-band mixing. Thus, coupling between $n_e \neq n_h$ (n_l) states is weakly allowed in these heterostructures, and we expect that our samples may show the existence of dark states at zero field. In Fig. 2(a), we display the zero field absorption spectra of $S1$ and $S2$ for excitation with σ^- polarization. Sample $S1$ shows no evidence of a dark state, while sample $S2$ shows a transition at 1.35 eV. Nonetheless, the absorption spectra
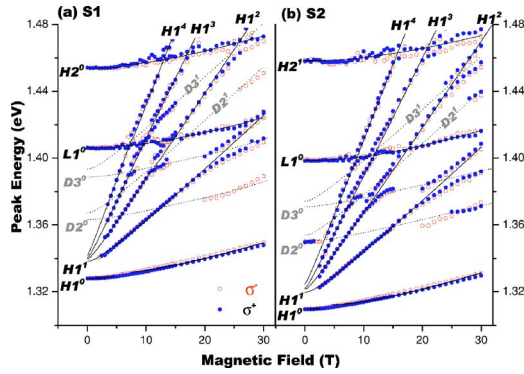
FIG. 3. (Color online.) Magnetoexciton spectral line positions in (a) $S1$ and (b) $S2$, for σ^+ (solid circle) and σ^- (hollow circle). The solid (dotted) lines depict the fitting curves of 2D magnetoexciton transitions for nominally allowed (forbidden) states.

FIG. 4. (Color online.) (a) Calculated prominent magnetoexciton states based on the modified Bauer-Ando model, showing anticrossings for the $H1^1$-$D3^0$ and $H1^2$-$D3^1$ lines. (b) Expanded view of the region around the $H1^1$-$D3^0$ anticrossing [shown as the box in (a)], comparing the experimental data (solid circles), valence band complexity (dashed line), and Coulomb interaction (solid light gray line).

of both samples indicate the presence of $D2^0$ at 30 T [Fig. 2(b)]. This occurs for both σ^- and σ^+. More importantly, the oscillator strength at 30 T for sample $S2$ is larger by a factor of 18 than the zero field case, much greater than would be expected by changes due to the magnetic field increase alone. The amplification of the dark state in $S2$ and its absence in $S1$ indicate that bright-dark mixing is a universal phenomenon in the $In_{0.2}Ga_{0.8}As/GaAs$ system.

Figure 3(a) shows the prominent exciton lines obtained from fitting the experimental data in Fig. 1(a) and 1(b). The filled (open) circles are obtained from measurements with σ^+ (σ^-) polarizations. $H1^5$, $H1^6$, $L1^1$, and $L1^2$ are omitted for clarity although they were experimentally observed. The solid lines in Fig. 3 are theoretical curves with reduced exciton mass μ, exciton binding energy E_X, and QW energy gap as fitting parameters while neglecting spin splitting and setting the dielectric constant ϵ at 11.61.[34] By comparing the excitonic Rydberg energy R_y^* to cyclotron energy $\hbar\omega_c$, the optically allowed transitions are fit using a hydrogenic (free Landau-level-like) exciton model for $\gamma < 1$ ($\gamma > 1$), where $\gamma = \hbar\omega_c/(2R_y^*)$.[23,35] The dotted lines correspond to the forbidden transitions with the inversion symmetry being preserved. The zero-field positions of $D2^0$ and $D3^1$ were confirmed from the estimated band structure including strain effects. $D2^n$ and $D3^n$ are interpolated over the whole range from experimental data, assuming an effective mass identical to $H1^n$. As indicated by the $D2^0$ line in Fig. 3(b) where the low-field data is well linked to high-field data, the assumption of the same effective mass is valid and can supply frames for tracing the *invisible* lines. Two features are noteworthy. First, our data show that $D3^0$ is well separated and not coupled to $L1^0$. Thus, it should not acquire "bright" character through valence-band mixing.[5,10] In addition, the Landau subbands of $H1^N$ are split into two lines below (above) $L1^0$ exactly around the $D3^0$ ($D3^1$) energy position, while the more optically active $D2^0$ and $D2^1$ do not affect the $H1^N$ subbands. Therefore, the splitting is sensitive to the parity of the dark and bright exciton branches.

The failure of a model incorporating valence band complexity to explain these anticrossings leads us to consider other mechanisms. There are two lines of evidence which suggest that the Coulomb interaction induces the splitting at
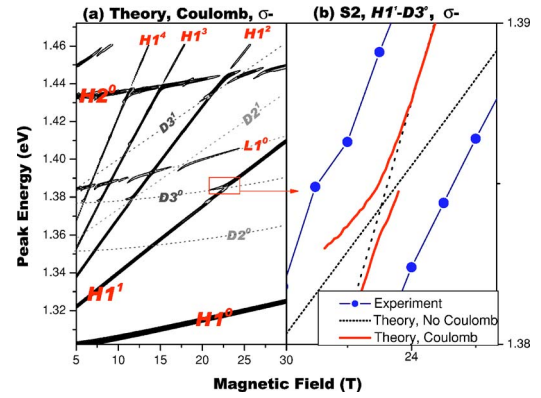
the mixing points. First, the incorporation of Coulomb interaction in our calculations (modified Bauer-Ando) leads to anticrossings in the predicted spectra. This can be seen in Fig. 4, where we present the results of our simulation of absorption spectra for sample $S2$. Figure 4(a) displays the field-dependent magnetoabsorption spectra over a magnetic field range of 30 T. Avoided crossings of the $H1^1$-$D3^0$ and $H1^2$-$D3^1$ lines are evident. Figure 4(b) compares the experimental data with both the Pidgeon-Brown and the modified Bauer-Ando models for the $H1^1$ and $D3^0$ states. In contrast to the 9 meV splitting exhibited in the experiment, the Pidgeon-Brown data shows no splitting. In contrast, the addition of the Coulomb interaction in the theory leads to an anticrossing in these states.

A second line of evidence comes from examining the character of the spectra at high carrier densities. Using a femtosecond pulsed laser source, we can excite high densities on short times scales before significant recombination can occur. Figure 5 displays field-dependent magnetophotoluminescence (MPL) spectra upon excitation by 775 nm, 150 fs pulses from a high power chirped pulse amplifier (CPA) at excitation intensities of 1.5 and 15 GW/cm^2. At these excitation powers, carrier densities of 4.5×10^{11} cm^2 [Fig. 5(a)] and 4.5×10^{12} cm^2 [Fig. 5(b)] are generated. As with the low density absorption spectra, the MPL spectra show various higher Landau-level states, but we do not observe any anticrossing even though clearly resolved higher LL states are visible. This is consistent with the mixing having a Coulombic origin. At high densities, the Coulomb interaction is screened out, and excitonic states are replaced with magnetoplasmonic behavior.[36]

The magnitude ($\sim$2 meV) of the predicted splitting is considerably smaller than the measured value of $\sim$9 meV. Thus, while our results identify the Coulomb interaction as important in the origin of the anticrossing, the large difference between the measured and theoretical energy splitting indicates that other mechanisms are also involved. One clue to the origin of the repulsive energy can be found by com-
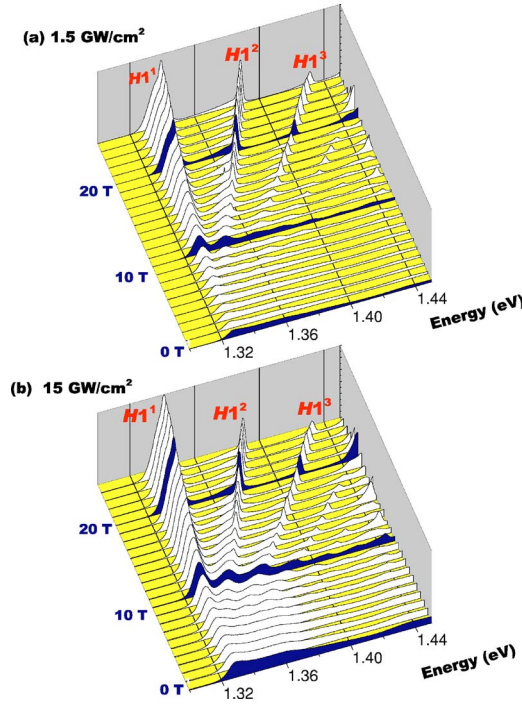
FIG. 5. (Color online.) Magnetophotoluminescence spectra obtained after excitation by high power femtosecond pulses at carrier densities of (a) 4.5×10^{11} cm^2 and (b) 4.5×10^{12} cm^2. In contrast to CW absorption spectra, no evidence of anticrossing behavior is seen.
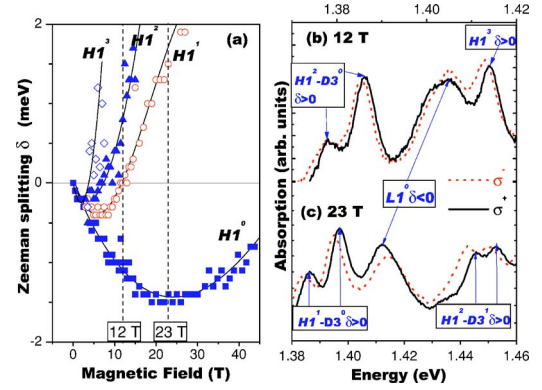

FIG. 6. (Color online.) (a) Field dependent Zeeman splitting for the $H1^N$ subbands. The solid lines are a guide to eye. At the fields denoted by dashed vertical line in (a), the individual σ^+ (solid lines) and σ^- (dotted lines) spectra are plotted for 12 T (b) and 23 T (c).

paring the magnitude of the anticrossing energy with the strain in each sample. Sample $S1$ (grown at the higher temperature) exhibits an HH-LH splitting of 78 meV at zero field with a measured $H1^1$-$D3^0$ splitting of 8.3 meV, while sample $S2$ has a HH-LH splitting of 89 meV and a $H1^1$-$D3^0$ level separation of 9.1 meV. In general the amount of uniaxial strain present in a system increases the HH-LH splittings. Thus, the larger splitting in $S2$ compared to $S1$ implies the correlation of the mixing strength with uniaxial strain and it is likely that strain plays a role in determining the splitting. It is important to emphasize, however, that the model including strain but not Coulomb effects predicts no level repulsion and thus strain is not solely responsible for the observed behavior.

In principle, there are a number of possible causes for the enhanced HH-LH splittings. The deviation of the magnetic field direction from the quantum well growth direction results in an in-plane component which can break the rotational symmetry of the Hamiltonian. While care was taken to ensure that the samples were mounted with the quantum growth directions parallel to the magnetic field axis to better than one degree, a misalignment of this magnitude produces an in-plane magnetic field component of approximately 0.4 T. In addition, any valence band warping breaks the rotational invariance and might be, in principle, responsible for anticrossing. However, based on the differences in the splittings for our samples and their correlation with growth temperature, we believe that the the presence of uniaxial strain in the planes of the quantum wells in our highly strained samples enhances the splitting caused by the Coulomb inter-

action between the excitons. This strain breaks the rotational symmetry of the problem (which was used in the Coulomb calculations) and may substantially increase the magnitude of anticrossing matrix elements.

IV. SPIN CHARACTER OF THE MIXED STATES

In addition to the optical character of the mixed states, our experiments also allow us to investigate how the mixed states "share" their spin (g-factor) character. Near the anticrossing point, the wave function ψ_{H1^N} mixes with $\psi_{D3^{N'}}$ to reveal a new set of wave functions:

$$\psi_1 = C_1 \psi_{D3^{N'}} + C_2 \psi_{H1^N}, \qquad (7)$$

$$\psi_2 = C_2 \psi_{D3^{N'}} - C_1 \psi_{H1^N}, \qquad (8)$$

where coupling coefficients C_1 and C_2, which are functions of the Coulomb interaction potential $V_{N,N'}$, are normalized to unity ($C_1^2 + C_2^2 = 1$). Since $\psi_{D3^{N'}}$ is optically inactive, the optical character of the new states $\psi_{1,2}$ preserves the identity of ψ_{H1^N} by sharing its original oscillator strength. Hence, they are polarized in the same way. We can describe their polarization state by examining the Zeeman splitting $\delta = E(\sigma^+) - E(\sigma^-) = -g_{ex} \mu_0 B$ between σ^+ and σ^- polarizations, where g_{ex} is the exciton g factor and μ_0 is the Bohr magneton. g_{ex} is the sum of effective hole g-factor g_h, which consists of valence-band Luttinger parameters,[37] and electron g-factor g_e.

Figure 6(a) shows measured δ for $H1^N$ transitions with N up to 3 for $S2$. The detailed shifts of δ for various coupled peaks are shown in Figs. 6(b) for 12 T and 6(c) 23 T. From Fig. 6(a), in all cases g_{ex} initially is negative and decreasing in value at low fields, reaching a minimum value and then increasing. Within a field range of 45 T, $H1^N$ levels with $N \geq 1$ show a sign reversal of g_{ex}. The field at which the sign change occurs scales roughly inversely with subband index N. That the spin character of the dark states arises from their bright companion can be seen by comparing the $H1^N$, $D3^{N'}$, and $L1^0$ peaks in Figs. 6(b) and 6(c). For the three mixed branches (1) $H1^2$-$D3^0$ [in Fig. 6(b)], (2) $H1^1$-$D3^0$, and (3)

$H1^2$-$D3^1$ [in Fig. 6(c)], the sign of $\delta\,(g_{ex})$ for mixed states follow $H1^N$, regardless of the subband index (N,N'). In contrast, the light holes $L1^0$ shift in the opposite direction, and thus possesses the opposite sign of g_{ex} in both cases. This further indicates that the mixing is obtained without interference from the LH excitons. These general features of the spin character were also observed in $S1$ but with different energy positions and HH-LH separations.

V. CONCLUSION

In conclusion, we have presented a systematic study of mixed states of dark and bright magnetoexcitons in strong magnetic field, wherein clear parity dependence was demonstrated. The polarization and parity dependencies are understood through a combination of Coulomb-interaction-mediated coupling between the same parity states as well as intrinsic strain. Qualitative agreements were achieved on mixing strengths and polarization dependencies of the mixed states. Field-dependent Zeeman splitting suggests that the spin character of the dark states comes from their bright exciton partners though the coupled states are a linear combination of dark and bright excitons whose energy variations are redefined through off-diagonal matrix terms in the Luttinger Hamiltonian.

[1] T. G. Eck, L. L. Foldy, and H. Wieder, Phys. Rev. Lett. **10**, 239 (1963).

[2] L. Viña, R. T. Collins, E. E. Mendez, and W. I. Wang, Phys. Rev. Lett. **58**, 832 (1987).

[3] G. E. W. Bauer and T. Ando, Phys. Rev. B **38**, 6015 (1988), and references therein.

[4] R. Magri and A. Zunger, Phys. Rev. B **62**, 10 364 (2000).

[5] R. C. Miller, A. C. Gossard, G. D. Sanders, Y. C. Chang, and J. N. Schulman, Phys. Rev. B **32**, R8452 (1985).

[6] L. W. Molenkamp, G. E. W. Bauer, R. Eppenga, and C. T. Foxon, Phys. Rev. B **38**, 6147 (1988).

[7] G. D. Sanders and Y. C. Chang, Phys. Rev. B **32**, 5517 (1985); **35**, R1300 (1987).

[8] L. Viña, L. Munoz, N. Mestres, E. S. Koteles, A. Ghiti, E. P. O'Rielly, D. C. Bertolet, and K. M. Lau, Phys. Rev. B **47**, R13926 (1993).

[9] G. D. Sanders, C.-K. Sun, J. G. Fujimoto, H. K. Choi, C. A. Wang, and C. J. Stanton, Phys. Rev. B **50**, 8539 (1994).

[10] W. M. Theis, G. D. Sanders, C. E. Leak, D. C. Reynolds, Yia-Chung Chang, K. Alavi, C. Colvard, and I. Shidlovsky, Phys. Rev. B **39**, R1442 (1989).

[11] G. Ortner, M. Bayer, A. Larionov, V. B. Timofeev, A. Forchel, Y. B. Lyanda-Geller, T. L. Reinecke, P. Hawrylak, S. Fafard, and Z. Wasilewski, Phys. Rev. Lett. **90**, 86404 (2003).

[12] S. Syed, M. J. Manfra, Y. J. Wang, H. L. Stormer, and R. J. Molnar, Phys. Rev. B **67**, 241304(R) (2003).

[13] J. Menéndez, A. Pinczuk, D. J. Werder, S. K. Sputz, R. C. Miller, D. L. Sivco, and A. Y. Cho, Phys. Rev. B **36**, R8165 (1987).

[14] K. F. Huang, K. Tai, S. N. G. Chu, and A. Y. Cho, Appl. Phys. Lett. **54**, 2026 (1989).

[15] R. C. Miller, D. A. Kleinman, W. T. Tsang, and A. C. Gossard, Phys. Rev. B **24**, R1134 (1981).

[16] R. L. Greene, K. K. Bajaj, and D. E. Phelps, Phys. Rev. B **29**, 1807 (1984).

[17] S. R. Eric Yang and L. J. Sham, Phys. Rev. Lett. **58**, 2598 (1987).

[18] A. Wojs, J. J. Quinn, and P. Hawrylak, Phys. Rev. B **62**, 4630 (2000).

[19] L. V. Butov, A. Zrenner, G. Abstreiter, A. V. Petinova, and K. Eberl, Phys. Rev. B **52**, 12 153 (1995).

[20] S. Glutsch, U. Siegner, M.-A. Mycek, and D. S. Chemla, Phys. Rev. B **50**, 17 009 (1994).

[21] C. K. Pidgeon and R. N. Brown, Phys. Rev. **146**, 575 (1966).

[22] G. D. Sanders, Y. Sun, F. V. Kyrychenko, C. J. Stanton, G. A. Khodaparast, M. A. Zudov, J. Kono, Y. H. Matsuda, N. Miura, and H. Munekata, Phys. Rev. B **68**, 165205 (2003).

[23] A. H. MacDonald and D. S. Ritchie, Phys. Rev. B **33**, 8336 (1986).

[24] J. M. Luttinger, Phys. Rev. **102**, 1030 (1956).

[25] See Eq. (1)–(17) of Ref. 22.

[26] H. Munekata (private communication).

[27] F. Bassani and G. P. Parravicini, *Electronic States and Optical Transitions in Solids* (Pergammon, New York, 1975).

[28] Y. P. Varshni, Physica (Amsterdam) **34**, 149 (1967).

[29] I. Vurgaftman, J. R. Meyer, and L. R. Ram-Mohan, J. Appl. Phys. **89**, 5814 (2001).

[30] W. Lamb, Phys. Rev. **85**, 259 (1952).

[31] L. P. Gor'kov and I. E. Dzyaloshinskii, Sov. Phys. JETP **26**, 449 (1968).

[32] R. S. Knox, *Theory of Excitons* (Academic Press, New York, 1963), p. 80.

[33] J. I. Pankove, *Optical Processes in Semiconductors* (Dover, New York, 1971).

[34] S. K. Cheung, H. Wang, W. Huang, and F. Jain, J. Appl. Phys. **81**, 497 (1997).

[35] O. Akimoto and H. Hasegawa, J. Phys. Soc. Jpn. **22**, 181 (1967).

[36] L. V. Butov, V. D. Egorov, V. D. Kulakovskii, and T. G. Andersson, Phys. Rev. B **46**, 15 156 (1992).

[37] M. J. Snelling, E. Blackwood, C. J. McDonagh, R. T. Harley, and C. T. B. Foxon, Phys. Rev. B **45**, R3922 (1992).